Z. Kristallogr. Suppl. **26** (2007) 461-466

Crystal Structure of the $Ba_3MgSi_2O_8:Mn^{2+},Eu^{2+}$ phosphor for white light emitting diodes

T. Aitasalo, A. Hietikko, J. Hölsä, M. Lastusaari*, J. Niittykoski, and T. Piispanen

University of Turku, Department of Chemistry, FI-20014 Turku, Finland
*Contact author; e-mail: miklas@utu.fi.

Keywords: Barium, disilicate, crystal structure, powder diffraction, LED

Abstract. The crystal structure of the $Ba_3MgSi_2O_8:Mn^{2+},Eu^{2+}$ phosphor for white light emitting diodes was observed to be trigonal with the space group $P\bar{3}$ (No. 147), *P321* (No. 150) or $P\bar{3}m1$ (No. 164), $Z = 1$, $a = 5.60909(1)$ and $c = 7.26655(1)$ Å based on X-ray powder diffraction data. No evidence for monoclinic merwinite type superstructure was found. The structure consists of two different Ba sites with 10- and 12- coordination and one 6-coordinated Mg. Moreover, the unit cell contains two crystallographically equivalent discrete SiO_4 tetrahedra with one O position with a 1/3 occupation.

Introduction

Silicates are good phosphor matrices because of their rigid and stable crystal structures. Materials like $CaSiO_3:Pb^{2+},Mn^{2+}$, $Y_2SiO_5:Ce^{3+}$, $Bi_4Si_3O_{12}$ and $Zn_2SiO_4:Mn^{2+}$ are used commercially in fluorescent lamps, cathode ray tubes, scintillators and plasma displays *etc*. Due to its narrow emission band in blue, the $Ba_3MgSi_2O_8:Eu^{2+}$ phosphor has been used for color correction in lamps, whereas the Mn^{2+}/Eu^{2+} co-doped material has found use in plant growth lamps [1]. In the recent few years, however, a number of patents and papers have been published about the use of $Ba_3MgSi_2O_8:Mn^{2+},Eu^{2+}$ as a phosphor for white LEDs [*e.g.* 2-4] needed to replace the inefficient conventional light bulbs and luminescent tubes that produce mercury waste.

In LEDs, the phosphors are required to absorb the primary UV or blue radiation emitted by the LED chip and convert it to visible light of desired color. The $Ba_3MgSi_2O_8:Mn^{2+},Eu^{2+}$ phosphor has a maximum at 375 nm in the excitation spectrum and it emits at 442 (blue), 505 (green) and 620 nm (red) [4] making it a good phosphor for white LEDs.

The crystal structure of $Ba_3MgSi_2O_8:Mn^{2+},Eu^{2+}$ has been assumed, based on a Rietveld refinement [4], to be merwinite ($Ca_3MgSi_2O_8$) type monoclinic, but no structural details or agreement index values have been reported. Merwinite crystallizes in the $P2_1/a$ (No. 14) space group with $Z = 4$ [5]. The structure is composed of MgO_6 octahedra linked at every corner by SiO_4 tetrahedra as well as one nine- and two eight-coordinated Ca atoms.

In this work, the crystal structure of $Ba_3MgSi_2O_8$ was studied based on powder diffraction data and analyzed by bond valence calculations.

Experimental

The polycrystalline doped and non-doped $Ba_3MgSi_2O_8$ samples were prepared with a solid state reaction of stoichiometric amounts of $BaCO_3$ (Merck, Pro Analysi), $Mg(NO_3)_2{\cdot}6H_2O$ (Merck, Pro Analysi) and fumed SiO_2 (Sigma, 99.8 %) using annealing for 5 h at 1250 °C in a reducing N_2 + 10 % H_2 gas sphere. The Mn^{2+} (x_{Mn} = 0.01 or 0.20 replacing Mg) and Eu^{2+} (x_{Eu} = 0.02 or 0.05 replacing Ba) dopants were introduced as $MnSO_4{\cdot}H_2O$ (Merck, Pro Analysi) and Eu_2O_3 (Treibacher Auermet, 99.99 %) in the mixture of the starting materials.
The X-ray powder diffraction patterns were measured at room temperature with a Huber 670 image plate (2θ range: 4-100°) Guinier camera using monochromatic copper $K_{\alpha 1}$ radiation (λ = 1.5406 Å). The dataset was summed from six 1/2 hour measurements. Preferred orientation was minimized by oscillating the sample horizontally.
The crystal structure determination was carried out by using the following programs: XFit [6] (peak search), Crysfire [7] (indexing), Chekcell [8] (space group search), Fox [9] (structure solution by direct space methods) and FullProf2k [10] (refinement).
The bond valences s_{ij} (in valence units, v.u.) [11] were calculated from the experimental bond lengths R_{ij} by using the tabulated bond valence parameters R_0 [12] and the empirical parameter B with an universal value of 0.37 [13] according to equation (1). The global instability index (*GII*) values compare the calculated bond valences and the formal valence (V_i) for all the species (N) in the asymmetric unit (equation 2) [14].

$$s_{ij} = exp[(R_0 - R_{ij})/B]. \quad (1)$$

$$GII = \sqrt{\sum_{i=1}^{N} [\sum_{j} (s_{ij} - V_i)^2 / N]}\,. \quad (2)$$

Crystal structure determination

The powder diffraction patterns of both $Ba_3MgSi_2O_8$ and $Ba_3MgSi_2O_8$:Mn^{2+},Eu^{2+} were observed to be rather similar to those in Ref. [4] and the Powder Diffraction File [15]. The only differences were observed in the intensities of some reflections between 25 and 30° in 2θ. Due to the strong variation of their intensities from one sample to another, it was found that these reflections were all due to orthorhombic Ba_2SiO_4 (space group *Pmcn*, No. 62, Z = 4 [16]), appearing as an impurity with different phase weights in all the samples in this work as well as in those in Refs. [4] and [15]. Moreover, no splitting of *e.g.* the intense reflection at 30.7° 2θ was observed. The structure could thus not be of the monoclinic merwinite type, since with a β angle differing from 90° the (402) and (411) reflections of the monoclinic cell would be split. A comparison with the pattern calculated based on the merwinite cell [5] but with β = 90°, shows the absence of the weak merwinite reflections, as well (Figure 1).
After the confirmation of the similarity of the patterns of the doped and non-doped samples that of non-doped $Ba_3MgSi_2O_8$ was indexed excluding the Ba_2SiO_4 reflections. The best observed/calculated reflections ratio of 22/36 was obtained with a trigonal or hexagonal cell

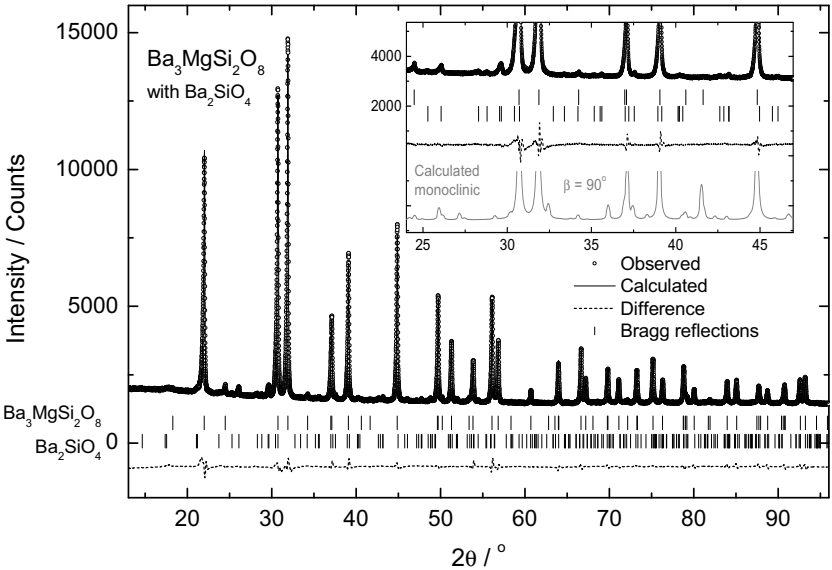

Figure 1. X-ray Rietveld plot of a two-phase refinement of $Ba_3MgSi_2O_8$ with Ba_2SiO_4. A calculated Ba-merwinite type pattern with $\beta = 90^o$ is given in the inset.

(a = 5.608 and c = 7.267 Å with Z = 1) and the sixteen trigonal and hexagonal space groups with no limiting reflection conditions. The unit cell dimensions were found very similar to those of glaserite, $K_3Na(SO_4)_2$ [17], whose crystal structure can be regarded as the idealized arrangement of that of merwinite [5]. Being 20 % larger than Ca^{2+} [18], Ba^{2+} is probably too large (r_{CN10} = 1.52 Å [18]) to form the dense merwinite cell [5], while it fits well to the K^+ sites (r_{CN10} = 1.59 Å [18]) of the glaserite one.

Since direct space methods using Fox [9] yielded no satisfactory values for the atomic positions in any of the sixteen space groups, the positions reported for $K_3Na(SO_4)_2$ [17] were used to start the Rietveld refinements in the space group $P\bar{3}\,m1$, instead. The structural similarity between $Ba_3MgSi_2O_8$ and $K_3Na(SO_4)_2$ as well as the total absence of superstructure reflections from the merwinite cell were then clearly observed (Figure 1).

A rather good fit was achieved, but the isotropic temperature factor of O1 assumed a high value of 7.5 $Å^2$ and a high *GII* value equal to 0.33 v.u. was obtained indicating that the structural model was not correct. Therefore, instead of the 2d (1/3, 2/3, z) position of glaserite, the O1 atom was considered to reside in the 6i (x, -x, z) position with 1/3 occupation. This yielded a fit with the *GII* value in agreement with the 0.20 v.u. of glaserite, but the B(O1) value was still rather high at 2.6 $Å^2$. However, this could be due to the high content of barium in the sample, which results in very little scattering power from the lighter atoms causing uncertainties in their positions. Next, the space group symmetry was lowered to *P321* (No. 150), which in the present case is equivalent to $P\bar{3}$ (No. 147), with both O1 and O2 at 6g (x, y, z) to yield a little lower *GII* value and the most realistic B values. However, the esd's for the coordinates of the O2 position as well as those of the bond lengths are clearly higher for

P321 than $P\bar{3}\,m1$ (Tables 1-3). Thus, both structural solutions with 1/3 occupation for the O1 site can be considered equally good, while the solution with O1 at the 2d position is clearly incorrect as indicated by the B parameter and *GII* values. Notice that the values of the conventional residual indices R_{wp}, R_B and χ^2 are similar for all three cases. The space group symmetry was finally lowered to *P3* (No. 143), but due to the lack of sufficient information in the diffraction pattern this gave no physically meaningful results.

Table 1. Unit cell parameters, atomic positions, site symmetries as well as residual and GII values for $Ba_3MgSi_2O_8$, Z =1.

Space group	$P\bar{3}\,m1$ (No. 164) (O1 at 2d)		$P\bar{3}\,m1$ (164) (O1 at 6i)		$P\bar{3}$ (147) or *P321* (150) (O1 at 6g)	
a in Å	5.60910(1)		5.60909(1)		5.60909(1)	
c in Å	7.26657(1)		7.26655(1)		7.26655(1)	
V in Å^3	197.99		197.99		197.99	
Ba1	2d (1/3, 2/3, z)	C_{3v}	2d (1/3, 2/3, z)	C_{3v}	2d (1/3, 2/3, z)	C_3
Ba2	1b (0, 0, 1/2)	D_{3d}	1b (0, 0, 1/2)	D_{3d}	1b (0, 0, 1/2)	S_6 / D_3
Mg	1a (0, 0, 0)	D_{3d}	1a (0, 0, 0)	D_{3d}	1a (0, 0, 0)	S_6 / D_3
Si	2d (2/3, 1/3, z)	C_{3v}	2d (2/3, 1/3, z)	C_{3v}	2d (2/3, 1/3, z)	C_3
O1	2d (1/3, 2/3, z)	C_{3v}	6i (x, -x, z)*	C_s	6g (x, y, z)*	C_1
O2	6i (x, -x, z)	C_s	6i (x, -x, z)	C_s	6g (x, y, z)	C_1
R_{wp} in %	2.9		2.9		2.9	
R_B in %	5.1		5.0		5.1	
χ^2	1.5		1.5		1.5	
GII (v.u.)	0.33		0.22		0.20	

* 1/3 occupation

Table 2. Atomic positions and isotropic temperature coefficients for $Ba_3MgSi_2O_8$.

Space group	$P\bar{3}\,m1$ (No. 164) (O1 at 2d)	$P\bar{3}\,m1$ (164) (O1 at 6i)	$P\bar{3}$ (147) or *P321* (150) (O1 at 6g)
z(Ba1)	0.17748(2)	0.17723(2)	0.17719(2)
B(Ba1) in Å^2	0.46(1)	0.43(1)	0.41(1)
B(Ba2) in Å^2	0.94(1)	1.04(1)	1.06(1)
B(Mg) /in Å^2	-0.12(2)	0.42(2)	0.53(2)
z(Si)	0.2515(1)	0.2559(1)	0.2571(1)
B(Si) in Å^2	1.12(1)	0.85(1)	0.76(1)
x(O1)	0.3333	0.2985(3)	0.2583(5)
y(O1)	0.6666	0.7015(3)	0.6541(9)
z(O1)	0.5316(2)	0.5268(2)	0.5264(2)
B(O1) in Å^2	7.48(5)	2.64(7)	1.31(7)
x(O2)	0.8214(1)	0.8213(1)	0.8238(50)
y(O2)	0.1786(1)	0.1787(1)	0.1781(50)
z(O2)	0.1697(1)	0.1717(1)	0.1717(1)
B(O2) /in Å^2	0.68(1)	0.76(1)	0.83(1)

Structural details

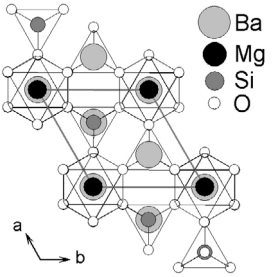

Figure 2. Unit cell of $Ba_3MgSi_2O_8$.

In contrast to $Ba_2MgSi_2O_7$ with MgO_4 tetrahedra and $[Si_2O_7]^{6-}$ units [19], the $Ba_3MgSi_2O_8$ structure contains discrete SiO_4 tetrahedra held together by MgO_6 octahedra to form layers of corner sharing polyhedra in the *ab* plane (Figure 2). The Ba1 atoms bond to 10 oxygens within the layers, while the Ba2 ones connect the layers by forming BaO_{12} polyhedra. The $M(2)O_{10}$ polyhedron has generally one rather short M-O distance (*e.g.* 2.547 Å for K-O in glaserite [17]), observed also in this work for Ba1-O1 (Table 3), which has been considered as a structural feature rather than a discrepancy. This short distance is observed also for merwinite [5], which possesses a quite distorted arrangement of the glaserite structure.

Table 3. Bond distances and angles for $Ba_3MgSi_2O_8$.

Distances in Å and Angles in °	$P\bar{3}\,m1$ (No. 164) (O1 at 2d)	$P\bar{3}\,m1$ (164) (O1 at 6i)	$P\bar{3}$ (147) or *P321* (150) (O1 at 6g)
Ba1-O1 x1	2.573(1)	2.563(1)	2.567(1)
Ba1-O2 x6	2.807(1)	2.807(1)	2.801(24) x3
			2.812(24) x3
Ba1-O2 x3	2.937(1)	2.947(1)	2.955(12)
Ba2-O1 x6	3.247(1)	2.907(1)	2.951(4)
Ba2-O2 x6	2.962(1)	2.950(1)	2.942(14)
<Ba1-O>	2.823	2.825	2.827
<Ba2-O>	3.104	2.940	2.947
<Ba-O>	2.976	2.881	2.892
Mg-O2 x6	2.129(1)	2.138(1)	2.126(20)
Si-O1 x1	1.576(2)	1.615(2)	1.621(2)
Si-O2 x3	1.617(1)	1.622(1)	1.639(22)
<Si-O>	1.607	1.620	1.635
O2-Mg-O2 x6	89.81(3)	89.38(3)	89.04(55)
O2-Mg-O2 x6	90.19(3)	90.62(3)	90.96(55)
O2-Mg-O2 x3	179.95(0)	180.00(0)	179.97(0)
O1-Si-O2	111.57(3)	100.06(6)	101.22(37)
O1-Si-O2	111.57(3)	117.77(7)	125.12(35)
O2-Si-O2	107.29(5)	106.65(5)	109.47(41)

According to the bond valence calculations, the M(2) atom is clearly the major contributor to the *GII* values of both $Ba_3MgSi_2O_8$ and $K_3Na(SO_4)_2$ indicating strains around the M(2) site. The *GII* values are at the empirically determined upper limit for stable structures (0.2 v.u. [14]) suggesting that both compounds may be instable. However, glaserite, that has its original Greek name (aphthitalite) owing to its stability in air, usually forms large crystal masses

and the stability of $Ba_3MgSi_2O_8$ in air exceeds 1300 ^oC. These facts contradict the suggestion of instability. Thus, this trigonal structure may be a too simple model, but the absence of superstructure reflections or reflection splitting gives no justification for going to any other unit cell or space group.

References

1. Shionoya, S. & Yen, W.M. (Eds.), 1999, *Phosphor Handbook* (Boca Raton FL, USA: CRC Press), pp. 391-394 & 414.
2. Ceintrey, C., LeMercier, T. & Wortham, E., 2005, *Fr. Demande*, Fr 2869159.
3. Chandran, R., Hancu, D., Mallikarjuna, N., Radkov, E., Setlur, A., Sivaramakrishan, V., Srivastava, A. & Shankar, M., 2006, *U.S. Pat. Appl. Publ.*, US 2006049414.
4. Kim, J.S., Leon, P.E., Choi, J.C., Park, H.L., Mho, S.I. & Kim, G.C., 2004, *Appl. Phys. Lett.*, **84**, 2931.
5. Moore, P.B. & Araki, T., 1972, *Amer. Mineral.,* **57**, 1355.
6. Coelho, A.A. & Cheary, R.W., 1997, *X-ray Line Profile Fitting Program, XFIT*, School of Physical Sciences, University of Technology, Sydney, Broadway, New South Wales, Australia.
7. Shirley, R., 2000, *The CRYSFIRE System for Automatic Powder Indexing: User's Manual* (Guilford, Great Britain: Lattice Press).
8. Laugier, J. & Bochu, B., 2002, *CHEKCELL, Powder Indexing Helper Tool for Unit Cell and Spacegroup Assignment*, LMGP, ENSP Grenoble (INPG), Domaine Universitaire, BP 46, F-38402 Saint Martin d'Hères, France.
9. Favre-Nicolin, V. & Cerny, R., 2002, *J. Appl. Cryst.,* **35***,* 734.
10. Rodriguez-Carvajal, J., 2005, *FullProf.2k (Version 3.40 November 2005)*, Laboratoire Leon Brillouin (CEA-CNRS), Gif-sur-Yvette, France, unpublished.
11. Zachariasen, W.H., 1978, *J. Less-Common Met.*, **62**, 1.
12. Brese, N.E. & O'Keeffe, M., 1991, *Acta Cryst.*, **B47**, 192.
13. Brown, I.D. & Altermatt, D., 1985, *Acta Cryst.*, **B41**, 244.
14. Salinas-Sanchez, A., Garcia-Muñoz, J.L., Rodriguez-Carvajal, J., Sáez-Puche, R. & Martinez, J.L., 1992, *J. Solid State Chem.*, **100**, 201.
15. JCPDS, 1997, *Powder Diffraction File*, entry No. 10-0074.
16. FIND IT v. 1.3.1, 2004, *FIZ/NIST Inorganic Crystal Structure Database*, Database December 2004, Fachinformationszentrum Karlsruhe, Germany, entry No. 6246.
17. Okada, K. & Ossaka, J., 1980, *Acta Cryst.*, **B36**, 919.
18. Shannon, R.D., 1976, *Acta Cryst.*, **A32**, 751.
19. Aitasalo, T., Hölsä, J., Laamanen, T., Lastusaari, M., Lehto, L., Niittykoski, J. & Pellé, F., 2006, *Z. Kristallogr. Suppl.*, **23**, 481.